Synthesis, Characterization, and Electrochemical Properties of $Ag_2V_4O_{11}$ and $AgVO_3$ 1-D Nano/Microstructures

*Shaoyan Zhang, Weiyang Li, Chunsheng Li, Jun Chen**

Institute of New Energy Material Chemistry, Nankai University, Tianjin 300071, P.R.China

*E-mail: chenabc@nankai.edu.cn

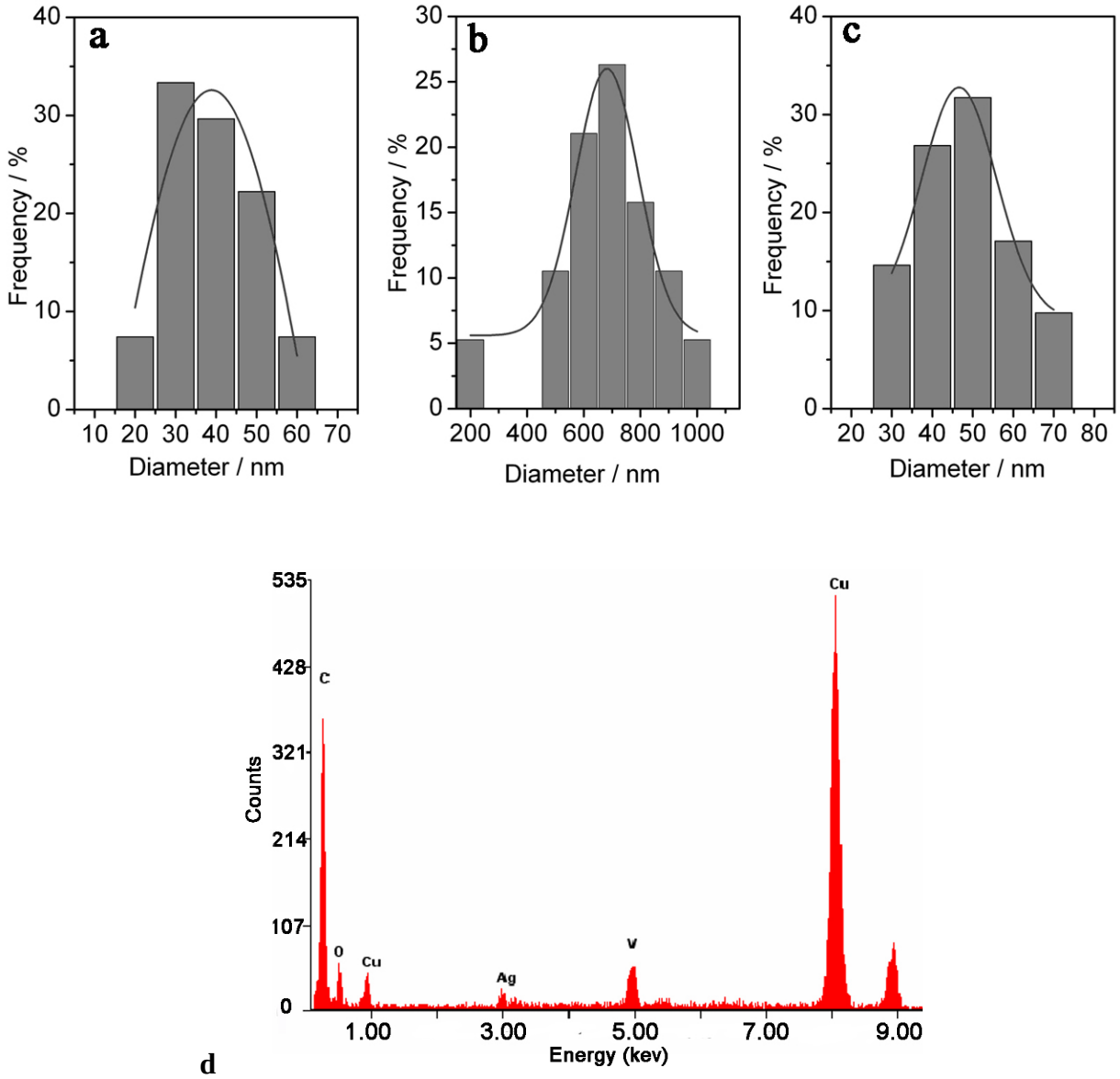

Figure S1. The statistic histogram of the as-prepared 1-D nano/microstructure diameters distribution: (a) $Ag_2V_4O_{11}$ nanowires, (b) α-$AgVO_3$ microrods and (c) β-$AgVO_3$ 1-D nanowires, which were measured on the basis of 100 nanowires or microrods in random regions. Curves are Gaussian fits. Means are 38.9, 681.7, and 46.6 nm and standard deviations are 2.4, 8.3, and 0.5 nm, respectively. (d)

The EDS analysis of the tiny nanoparticle on the nanowire in Figure 2d.

It is found that the morphology of the as-synthesized β-$AgVO_3$ was dramatically influenced by the initial pH of the precursor mixture of the NH_4VO_3 and $AgNO_3$ solution prior to the hydrothermal treatment. β-$AgVO_3$ nanowires with a diameter of 40−50 nm, as shown in Figure 3c−f, were obtained when the pH of the precursor mixture was maintained to be approximately 5. When the pH was adjusted to 6-8 with dilute $NH_3 \cdot H_2O$, the product was microrods with a diameter of 200−500 nm, as demonstrated by the SEM image in Figure S1. The results indicate that the diameter of the 1-D β-$AgVO_3$ nano/microstructures can be simply controlled in the range of 40 nm−1 μm by altering the pH of the precursor mixture.

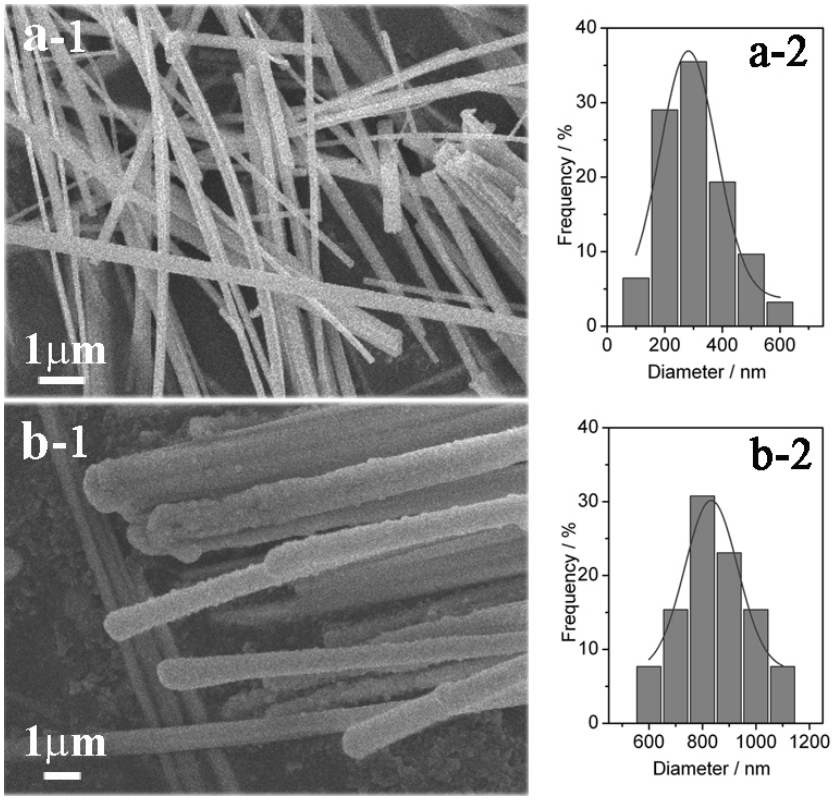

Figure S2. SEM images and the diameters distribution of β-$AgVO_3$ microrods obtained at different pH value: (a) pH = 6, (b) pH = 8. The statistic histograms of the diameters distribution were measured on

the basis of 100 microrods in random regions. Curves are Gaussian fits. Means are 282.3 and 832.7 nm and standard deviations are 11.3 and 13.9 nm, respectively.

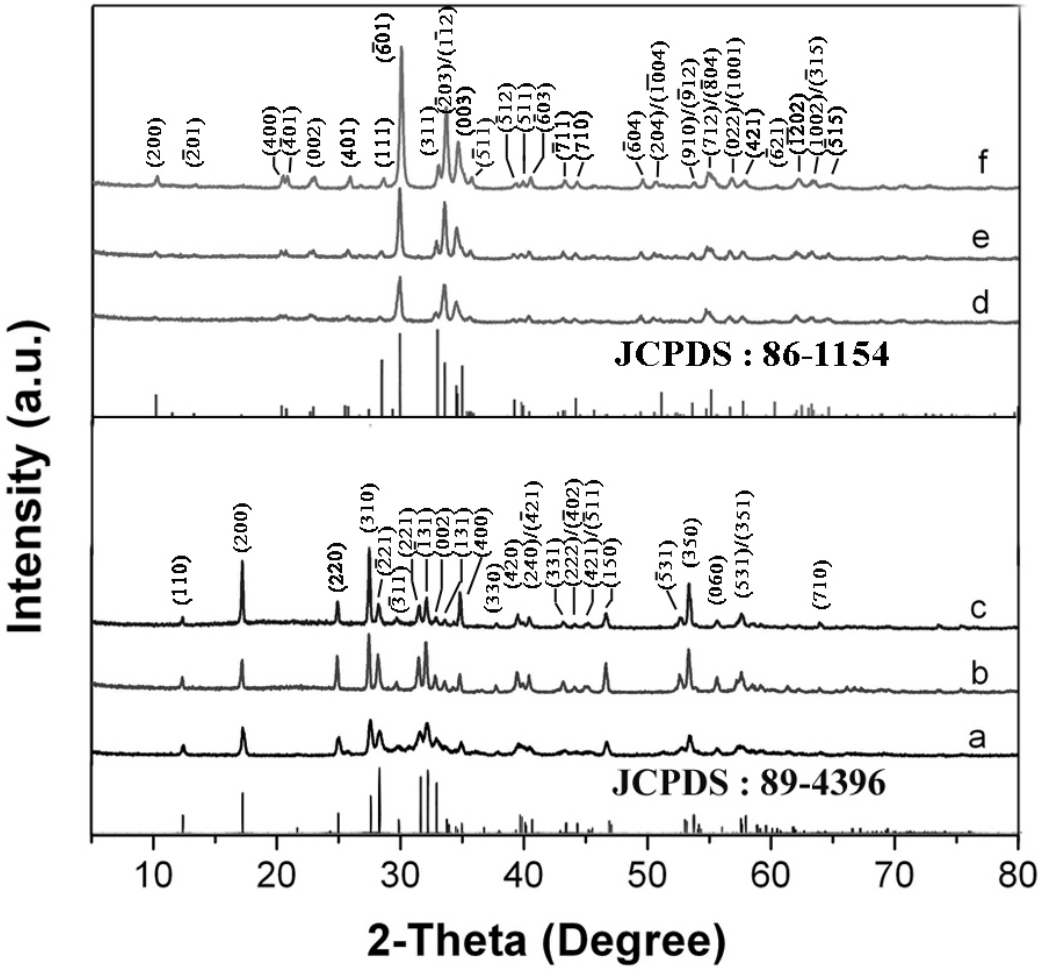

Figure S3. XRD patterns of $AgVO_3$ obtained at different hydrothermal dwell time. (a) 0 h, (b) 2 h, (c) 4 h, (d) 6 h, (e) 8 h, and (f) 15 h.

Initially, the direct mixing of the $AgNO_3$ and NH_4VO_3 solution immediately led to the formation of an orange precipitate. The morphology of the orange precipitate before the hydrothermal process was shown to be a coexistence of irregular particles and short rods (Figure S4a). After the precipitate was

hydrothermally treated at 180 ºC for 2 h, irregular particles vanished and longer rods formed (Figure S4b). When the dwell time was increased to 4 h, α-$AgVO_3$ microrods (Figure 3a and b) were obtained. Interestingly, it is noticed that the microrods began to split into nanowires (Figure S4c and d) as the reaction time was extended to 6 h, which corresponds to the time when α-$AgVO_3$ transformed to β-$AgVO_3$. Then the proportion of the nanowires in the product increased with increased reaction time (Figure S4e and f), and finally the product became β-$AgVO_3$ nanowires after 15 h, as demonstrated in Figure 3c and d.

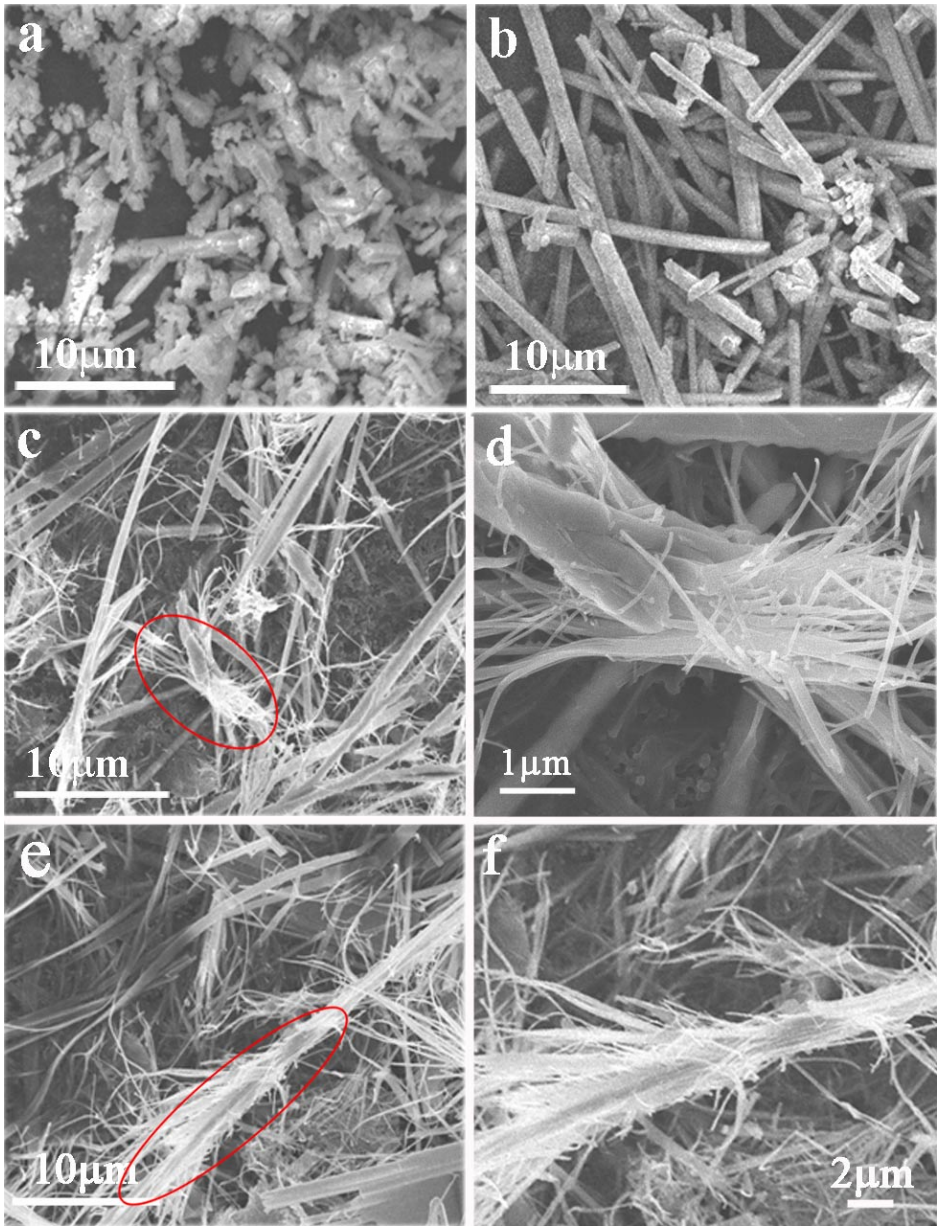

Figure S4. SEM images of $AgVO_3$ obtained at different hydrothermal dwell time: (a) 0 h, (b) 2 h, (c, d) 6 h, and (e, f) 8 h.

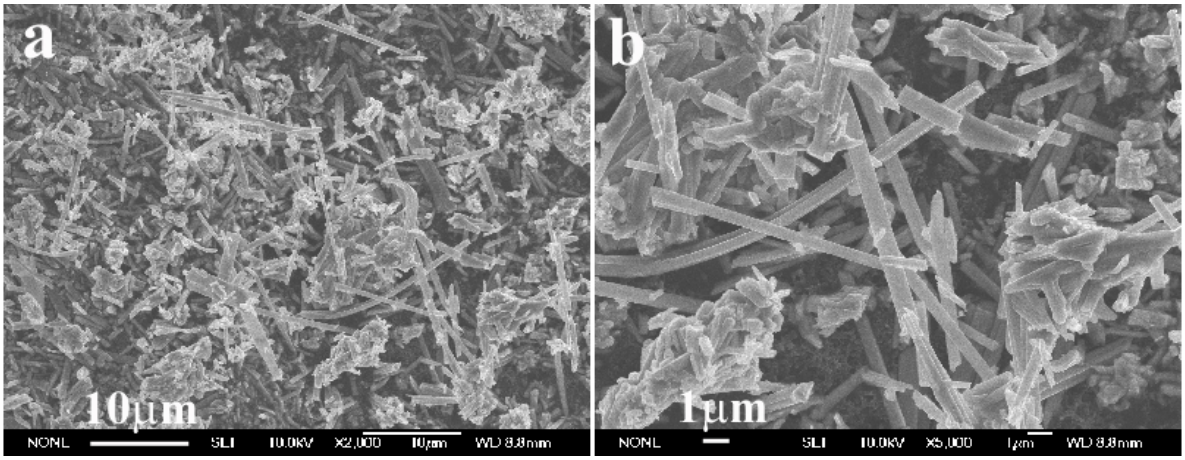

Figure S5. SEM images of $Ag_2V_4O_{11}$ bulk particles obtained from solid-state reaction at (a) a lower and (b) a higher magnification.

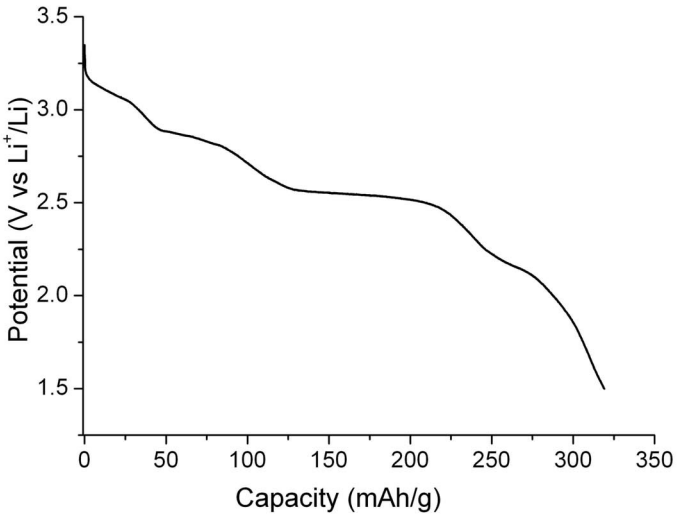

Figure S6. Discharge curves as a function of capacity for the electrode made from the as-prepared $Ag_2V_4O_{11}$ bulk particles at the current density of 0.01 mA and the temperature of 37 ^oC.

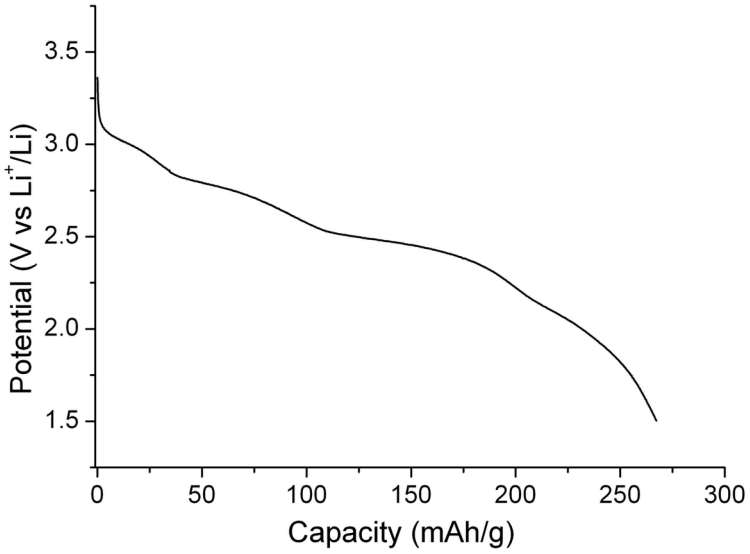

Figure S7. Discharge curves as a function of capacity for the electrode made from the as-prepared $Ag_2V_4O_{11}$ bulk particles at the current density of 0.1 mA and the temperature of 37 ^oC.

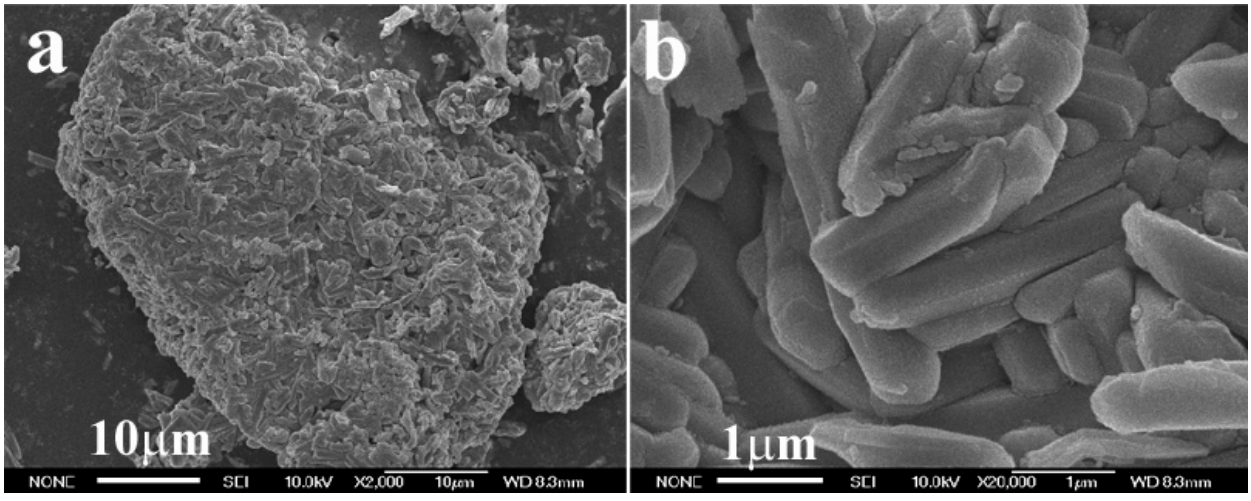

Figure S8. SEM images of β-$AgVO_3$ bulk particles obtained from solid-state reaction at (a) a low and (b) a higher magnification.

The formation of silver in the discharge process was further confirmed by the XRD measurement. Figure S9 shows the XRD patterns of α-$AgVO_3$ microrods and β-$AgVO_3$ nanowires after discharging to the cut-off voltage of 1.5 V. It was observed that the characteristic diffraction peaks corresponding to α- and β-$AgVO_3$ vanished, and a group of strong diffraction peaks are found at 2θ = 38.1, 44.3, 64.4, and 77.4˚, which can be attributed to metallic silver, in accordance with the results in the XPS. The diffraction peak appearing at 2θ = 18.0˚ can be assigned to the binding agent PTFE used during the fabrication process of the electrodes (Figure S10). The disappearance of the diffraction peaks for α- or β-$AgVO_3$ may be due to the destruction of the host lattice caused by the insertion of lithium during the discharge process. A loss in crystallinity with lithiation was also observed for $Ag_2V_4O_{11}$ and $Ag_{1.2}V_3O_8$.

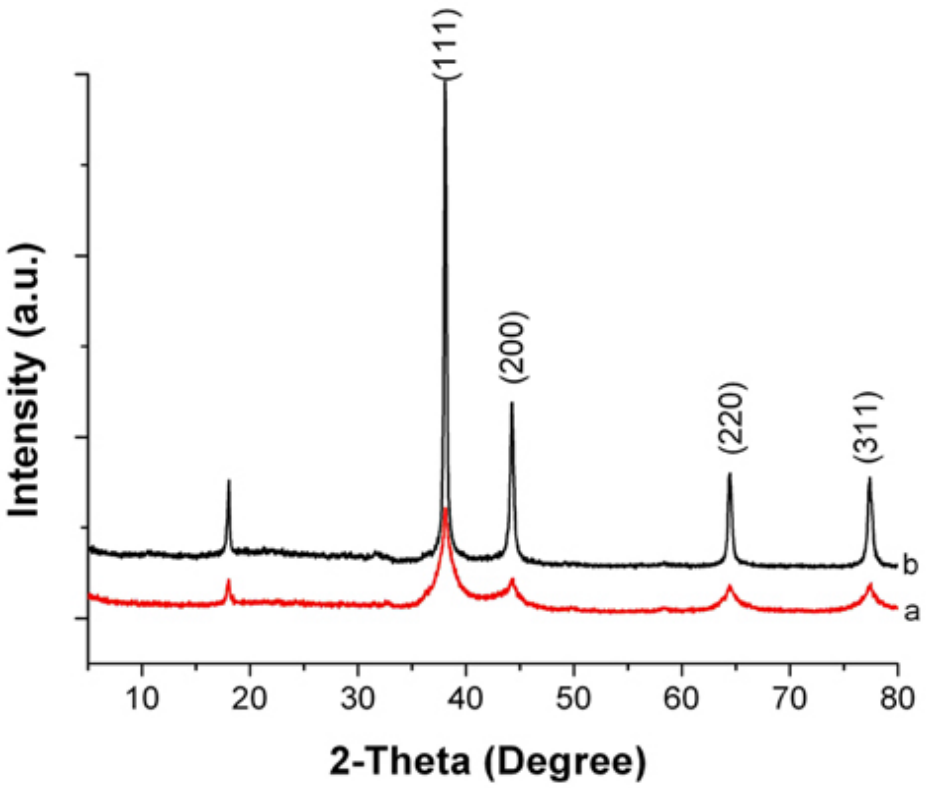

Figure S9. XRD patterns of (a) α-$AgVO_3$ microrod and (b) β-$AgVO_3$ nanowire electrodes after discharging to the cut-off voltage of 1.5 V.

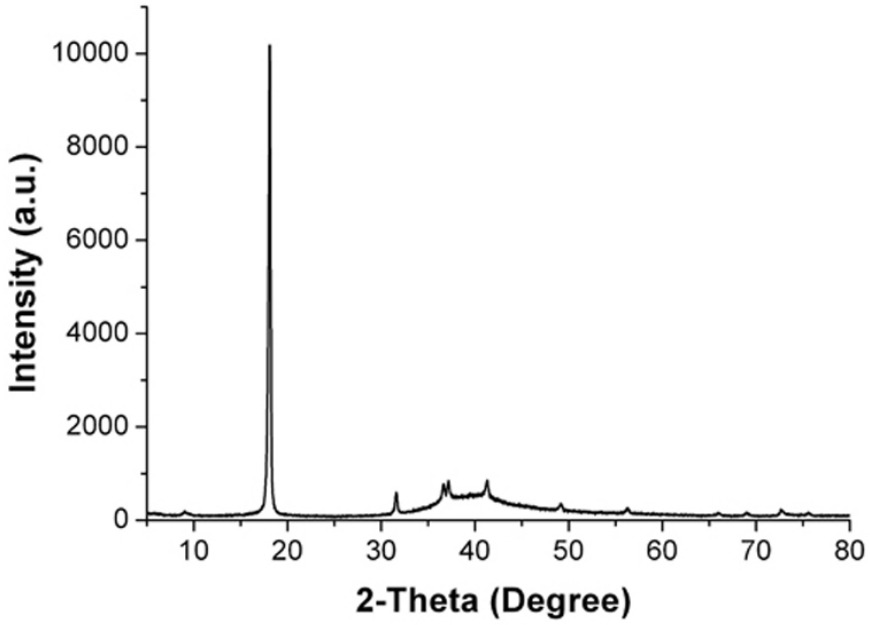

Figure S10. XRD pattern of the PTFE used in the fabrication of the electrodes. [JCPDS-ICDD Card No. 47-2217]

Table S1. Comparison of the cathode materials used in rechargeable lithium ion batteries.

Cathode material	Capacity (mAh g^{-1})
$LiCoO_2$	155
$LiNiO_2$	200
$LiMn_2O_4$	120
$LiFePO_4$	160
TiS_2	226
$Ag_2V_4O_{11}$	315